Efficiency of a Vertical Axis Wind Turbine (VAWT) with Airfoil Pitch Control

Junkun Ma[*1], Cris Koutsougeras[2], and Hao Luo[2]
[1]Sam Houston State University, [2]Southeastern Louisiana University
*Corresponding author: Junkun Ma, Sam Houston State University, Department of Agricultural Sciences & Engineering Technology, Box 2088, Huntsville, TX 77341-2088, USA. Email: jxm158@shsu.edu

Abstract: This paper presents a study of the effects of airfoil pitch control on the fluid dynamics and efficiency of a Vertical Axis Wind Turbine (VAWT) with airfoil that pivots freely with respect to its supporting arm attached to the main shaft of the VAWT. The steady-state velocity and pressure fields for different airfoil pivoting angles at a series of VAWT rotation angles are obtained. Net force on the airfoil at a given position, which is directly related to the efficiency of the VAWT, is also derived based on the pressure field and the airfoil geometry. As a comparison, wind speeds representing both laminar and chaotic air flows are considered. The results show that an optimal airfoil pivoting angle resulting in maximum net force exists at any given VAWT rotation angle. It is also shown that the maximum net force at a given VAWT rotation angle increases non-linearly as the wind speed increases.

Keywords: Vertical Axis Wind Turbine (VAWT), pitch control, efficiency.

1. Introduction

As a type of wind turbine where the rotor shaft is placed vertically, a vertical axis wind turbine (VAWT) is easier to install and maintain since the generator and clutch can be placed at the bottom of a VAWT where it is close to the ground. One additional benefit of this setup is that there is no need to point it into the wind [1]. Despite these advantages, starting from the early lift-based Darrieus[2] rotors and later cycloturbines[3] to drag-based Savonius rotor[4], VAWT has been facing many challenges including low starting torque, low peak efficiency, narrow operating range, pulsatory torque, and dynamic stability problems. Some derived rotors such as the Giromills design[5] and the Helical blades[6] can help improve one disadvantage (such as low starting torque) but usually at the sacrifice of another advantage (such as high peak efficiency). Researchers later suggested pitch control systems such as the Self- Sinusoidal Forced Pitch Variation[7] and the Acting Stabilized Pitch Control[8] for performance improvement. Experimental results have shown that they all have improved starting torque, broader operating range and higher efficiency when compared to the aforementioned fixed pitch VAWTs[9]. Recently, a dynamic control system includes both pitch and camber controls is presented[10]. Figure 1 shows the schematic (top view) of such a system consisting of three blades with flaps at the trailing edge. Each blade is supported by the blade supporting arm which is attached to the vertical axis via the hub as shown. Using individual actuators, pitch control of each blade can be achieved by rotating the blades around their own blade pivot point, while camber control is achieved by rotating the trailing edge flap around the pivoting point between the blade airfoil and the flaps. Power extraction improvements of the system as a result of employing both pitch and camber control have been reported [10].

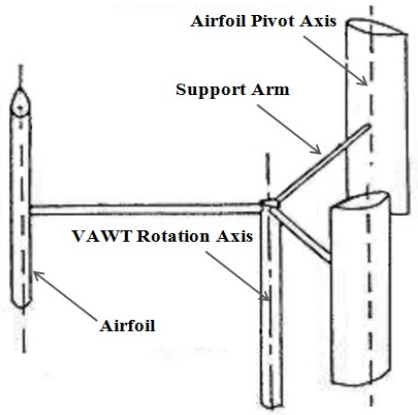

Figure 1. Schematic of a VAWT consisting three airfoils with pitch control

The main objective of this study is to determine the pressure field on the airfoil surface and based on the pressure field properties to then develop an optimal airfoil pitch control pattern as the VAWT rotating for maximum energy output. As a first approach, a series of 2D models representing various wind angle of attacks (thus airfoil pivot angles) ranging from 0^0 to 180^0 with

10^0 increments of a single airfoil are created and simulated using the COMSOL CFD™ module. To determine possible effects of wind speed, initial wind speeds of 5m/s and 10m/s representing laminar flow, as well as 15m/s and 20m/s representing turbulent flow are also investigated. The NACA 0012 airfoil as shown in Figure 2 is chosen for this study.

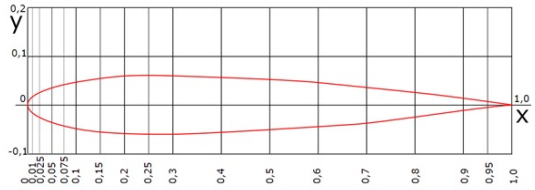

$$y = \pm 0.6[0.2969\sqrt{x} - 0.1260x - 0.3516x^2 + 0.2843x^3 - 0.1015x^4]$$

Figure 2. NACA 0012 airfoil

2. Governing Equations

2.1 Overview

For the purpose of this study, wind is considered to be a homogeneous mass (no dust, vapor or other particles), and no shear is assumed. Thus, at low wind speed, the modeling is based on single phase flow, which is modelled by the Navier-Stokes fluid flow equations. For high wind speed, by calculating the Reynolds number, it is determined that the wind entered the laminar separation/turbulent transitional flow. The k-ε model is used for this purpose.

2.2 Low speed laminar flow

The general form of Navier-Stokes equations for single phase fluid flow can be expressed as the follows.

$$\frac{\partial \rho}{\partial t} + \nabla \cdot (\rho \boldsymbol{u}) = 0$$

$$\rho \frac{\partial \boldsymbol{u}}{\partial t} + \rho(\boldsymbol{u} \cdot \nabla)\boldsymbol{u} = \nabla \cdot [-p\boldsymbol{I} + \boldsymbol{\tau}] + \boldsymbol{F}$$

$$\rho C_p \left(\frac{\partial T}{\partial t} + (\boldsymbol{u} \cdot \nabla)\boldsymbol{T}\right) = -(\nabla \cdot \boldsymbol{q}) + \boldsymbol{\tau} : \boldsymbol{S} - \frac{T}{\rho}\frac{\partial \rho}{\partial T}|_p \left(\frac{\partial p}{\partial t} + (\boldsymbol{u} \cdot \nabla)p + \boldsymbol{Q}\right)$$

where:

- ρ is the density (SI unit: kg/m^3)
- $\boldsymbol{u}$ is the velocity vector (SI unit: m/s)
- $\boldsymbol{p}$ is pressure (SI unit: Pa)
- $\boldsymbol{\tau}$ is the viscous stress tensor (SI unit: Pa)
- $\boldsymbol{F}$ is the volume force vector (SI unit: N/m^3)
- $\boldsymbol{C_p}$ is the specific heat capacity at constant pressure (SI unit: $\mathrm{J}/(\mathrm{kg} \cdot \mathrm{K})$)
- T is the absolute temperature (SI unit: K)
- $\boldsymbol{q}$ is the heat flux vector (SI unit: W/m^2)
- $\boldsymbol{Q}$ contains the heat sources (SI unit: W/m^3)
- $\boldsymbol{S}$ is the strain-rate tensor:

$$\boldsymbol{S} = \frac{\boldsymbol{1}}{\boldsymbol{2}}(\nabla \boldsymbol{u} + (\nabla \boldsymbol{u})^T)$$

The equations in the group represent conservation of mass, conservation of momentum, and conservation of energy accordingly. The operator ':' denotes a contraction between two tensors. In this study, air flow through the airfoil is considered isothermal.

2.3 High speed turbulent flow

A fundamental parameter in fluid dynamics is the Reynolds number (Re), which is defined as the follow and is used to identify characteristics and form of fluid flow.

$$Re = \frac{\rho U L}{\mu}$$

where U is the magnitude of fluid velocity, and L is the representative length of the object. Considering the operating condition of these VAWT included wind speeds up to 25m/s and possible interaction between multi-airfoils, turbulent flow is also considered. For the NACA0012 airfoil used in this study, given air density ρ =1.29kg/m^3, highest wind speed U = 20.0m/s, airfoil chord length L = 1.0m, air viscosity μ = 18.1×10^{-5}$kg/(m.s)$, the Re number at these conditions is approximately 1.39×10^5 indicating turbulent air flow.

The most commonly used k-ε model for turbulent flow adds two additional parameters: the turbulent kinetic energy k and the turbulent dissipation rate ε. The turbulent viscosity is modeled as follows:

$$\mu_T = \rho C_\mu \frac{k^2}{\varepsilon}$$

where C_μ is a model constant. The transport equation for turbulent kinetic energy k is represented as follows:

$$\rho \frac{\partial k}{\partial t} + \rho u \cdot \nabla k = \nabla \cdot \left(\left(\mu + \frac{\mu_T}{\sigma_k}\right)\nabla k\right) + P_k - \rho\varepsilon$$

The product term in the above equation is expressed as:

$$P_k = \mu_T \left(\nabla \boldsymbol{u} : (\nabla \boldsymbol{u} + (\nabla \boldsymbol{u})^T) - \frac{2}{3}(\nabla \cdot \boldsymbol{u})^2\right) - \frac{2}{3}\rho k \nabla \cdot \boldsymbol{u}$$

The transport equation for the turbulent dissipation rate ε is represented as the following.

$$\rho \frac{\partial \varepsilon}{\partial t} + \rho \boldsymbol{u} \cdot \nabla \varepsilon = \nabla \cdot \left(\left(\mu + \frac{\mu_T}{\sigma_\varepsilon}\right)\nabla \varepsilon\right) + C_{\varepsilon 1}\frac{\varepsilon}{k}P_k - C_{\varepsilon 2}\rho\frac{\varepsilon^2}{k}$$

The constants in these equations are determined from experimental results and the values are listed in the Table 1 shown below.

CONSTANT	VALUE
C_μ	0.09
$C_{\varepsilon 1}$	1.44
$C_{\varepsilon 2}$	1.92
σ_k	1.0
σ_ε	1.3

Table 1. Constants in the *k-ε* turbulent flow model

2.4 Force on airfoil and corresponding torque

Using the models described in the above sections, the air velocity and pressure fields around the airfoil for various VAWT rotation angles and airfoil pivot angles can be obtained. The total force acting on the airfoil surface can be calculated by integrating the force vector over the airfoil surface. For the 2D case in this study, it can be computed as follows:

$$\vec{F} = \oint d\vec{F} = \oint \vec{p} * ds$$

where *ds* is an indefinitely small section along the airfoil surface, and $\vec{p}$ is the pressure vector acting on the *ds*, which can be expressed as $\vec{p} = p * (-\vec{n})$, where p is the magnitude of the pressure on the *ds*, which is obtained from the COMSOL simulation, and $\vec{n}$ is the unit vector along the normal direction of the *ds* segment. As shown in Figure 1, the surface contour of the airfoil is determined by the following function.

$$y = \pm 0.6\left[0.2969\sqrt{x} - 0.126x - 0.3516x^2 + 0.2843x^3 - 0.1015x^4\right]$$

The tangential slope $k_t = y'(x)$, and normal slope $k_n = -1/k_t = -1/y'(x)$ at any given location (*x*, *y*) on the airfoil can be calculated. Subsequently, the unit vector $\vec{n}$ along the normal direction of the *ds* segment and the corresponding force vector $\vec{F}$ due to pressure $\vec{p}$ can be found as follows ($\vec{\imath}$ and $\vec{\jmath}$ are the unit vectors of the coordinate system).

$$\vec{n} = \frac{1}{\sqrt{1^2 + (-1/y'(x))^2}}\vec{\imath} + \frac{-1/y'(x)}{\sqrt{1^2 + (-1/y'(x))^2}}\vec{\jmath}$$

$$\vec{F} = \oint p * \frac{-1}{\sqrt{1^2 + (-1/y'(x))^2}} * ds\vec{\imath} + \oint p * \frac{1/y'(x)}{\sqrt{1^2 + (-1/y'(x))^2}} * ds\vec{\jmath}$$

Consequently, the torque with respect to the VAWT rotation center due to the pressure on the airfoil can be obtained.

$$\vec{T} = \oint d\vec{T} = \oint \vec{r} \otimes d\vec{F}$$

where $\vec{r}$ is the vector from the VAWT rotation center to the *ds* segment on which the $d\vec{F}$ is acting on.

3. Numerical Model

3.1 Use of COMSOL CFD

The COMSOL CFD module is extensively used to model and simulate both the velocity and the pressure fields around the NACA 0012 airfoil at different airfoil pivot angles (wind angle of attacks) for wind speeds spanning the range from laminar flow to turbulent flow. The 'Line Integration' feature which allows input of customized integration function in the 'Results' post-processing module is extremely helpful and makes it easy to calculate the total net force and corresponding torque. The results show that an optimal airfoil pivot angle for maximum torque exists at a given VAWT rotation angle providing a guideline for airfoil pitch control.

3.2 COMSOL CFD Model

The 2-D geometry of the NACA 0012 airfoil was developed using the COMSOL Multi-Physics graphics user interface. It is then placed in a rectangle area (10 meters long by 4 meters wide) representing a section of a wind tunnel. The top and bottom edges of the rectangle area as well as the surface of the airfoil are set as wall boundary condition, while the left and right edges of the rectangle are set as inlet where wind flows in uniformly along the horizontal direction and outlet correspondingly. In this study, the airfoil chord length was set to one meter (*x* in the airfoil function described in section 2.4 changes from 0 to 1). Figure 3 shows a schematic representation of the models used in this study.

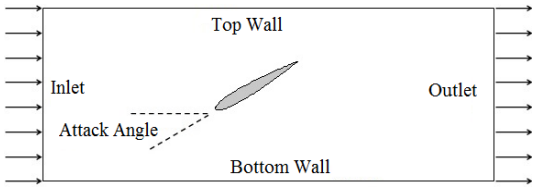

Figure 3. COMSOL CFD Model

As described in section 2.4, to find the net force and corresponding torque, it is necessary to

conduct line integration over the surface of the airfoil. The function determining the surface contour of the NACA 0012 airfoil as shown in Figure 2 is valid only when the chord of the airfoil is horizontal. In the case that the airfoil is rotated, this function will change.

To avoid the calculation of airfoil function after rotation as well as the subsequent derivation of normal direction and force vector along the airfoil surface, airfoils are fixed along the horizontal direction. Instead, the rectangle box representing a section of a wind tunnel is rotated. As long as the wind speed is specified as perpendicular to the inlet edge, the same wind angle of attack can be achieved. Figure 4 shows the meshed geometry for a 30^0 rotated airfoil. The upper left edge of the rectangle is the inlet boundary condition. (The mesh in Figure 4 is for illustration purpose. The actual mesh used for the simulation is much finer)

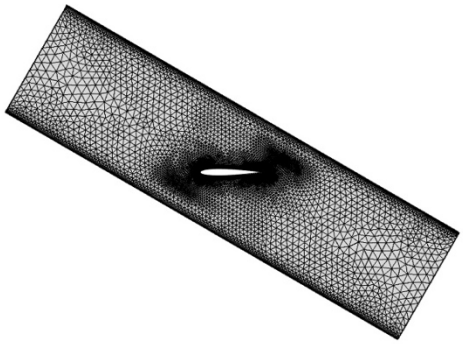

Figure 4. A 30^0 rotated airfoil model

4. Results and Discussion

A series of 2-D models representing varying airfoil pivot angle (represented by the angle of attack as shown in Figure 5) ranging from 0^0 to 180^0 with 10^0 increment at a given support arm position (represented by the support arm angle as shown in Figure 5) are created. Support arm angle is also changed from 0^0 to 180^0 with 10^0 increment. Wind speeds of 5m/s, 10m/s, 15m/s, and 20m/s representing both laminar and turbulent flow are also considered. The effects of these factors on the fluid flow, pressure distribution on the airfoil surface, and torque with respect to the VAWT rotation center are investigated. The goal is to find out the optimal pivot angle for any given support arm position so that the maximum torque at that position can be achieved. Selected results are presented below.

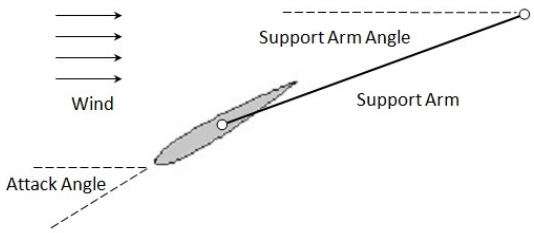

Figure 5. Definition of attack and support arm angles

4.1 Velocity profile

The velocity profiles of an airfoil positioned at 30^0 angle of attack and subjected to 20m/s wind as shown in Figure 4 are shown in Figure 6 (whole field) and Figure 7 (field near the airfoil). The magnitude of velocity along the top and bottom surfaces of the airfoil is shown in Figure 8. The maximum air flow speed reaches 35.6m/s and it reaches the maximum at near the leading edge of the airfoil, while the minimum air flow speed is 0.02m/s and it is located at near the leading edge on the bottom side of the airfoil. Other airfoil rotation angles show similar air flow behavior.

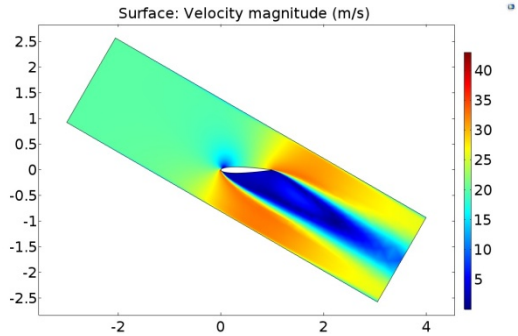

Figure 6. Velocity field at 30^0 angle of attack

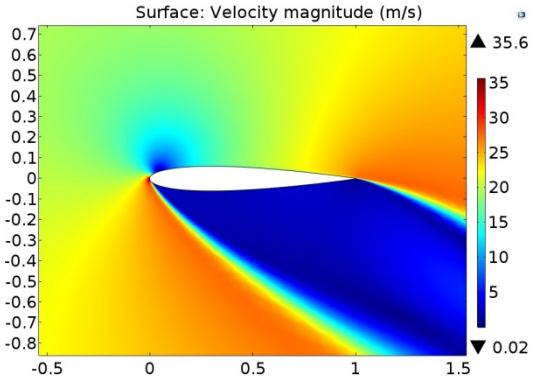

Figure 7. Velocity field close up at 30^0 angle of attack

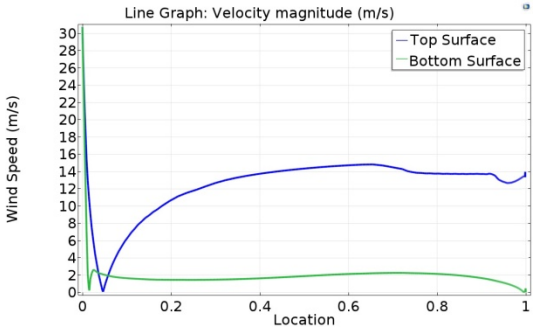

Figure 8. Velocity on the airfoil surfaces

4.2 Pressure profile

The pressure profiles for the same example discussed in the previous section are shown in Figure 9 (whole field) and Figure 10 (field near the airfoil). Figure 11 also shows the pressure distribution on the top and bottom surfaces of the airfoil. It is shown that the peak pressure occurs at near the leading edge on the top of the airfoil where the lowest flow speed exists. Where the lowest pressure exists at near the leading edge on the bottom of the airfoil where the highest flow speed is.

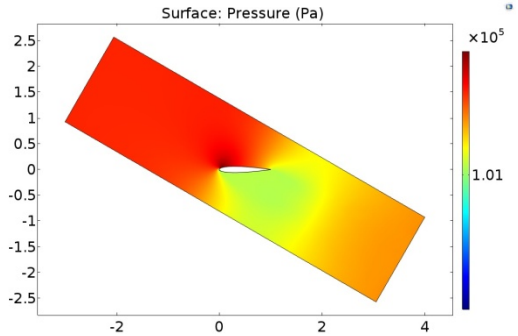

Figure 9. Pressure field at 30^0 angle of attack

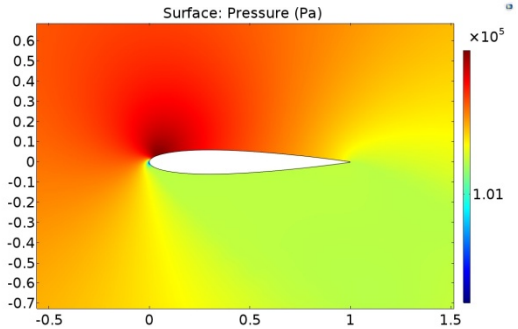

Figure 10. Pressure field close up at 30^0 angle of attack

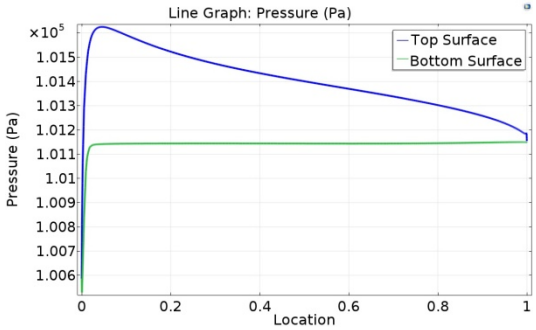

Figure 11. Pressure on the airfoil surfaces.

The peak pressure increases from 1atm (1.0133E5 Pa) to 1.0173E5 Pa and the lowest pressure drops to 1.0021E5 Pa. Both velocity and pressure on the bottom of the airfoil remain nearly constant with the exception of change at near the leading edge.

4.3 Torque

As described in section 2.4, torque with respect to the rotation center of a VAWT can be derived from the pressure field on the airfoil surface. As an example, Figure 12 shows how torque changes when the angle of attack changes for the case where the support arm angle is 30^0 and wind speed equals to 20m/s. The figure shows that the torque increases as the angle of attack increases from 0^0, and reaches peak value at 90^0. The torque starts to drop as the angle of attack keeps increasing beyond 90^0, and return back to similar level as that when the angle of attack is 0^0.

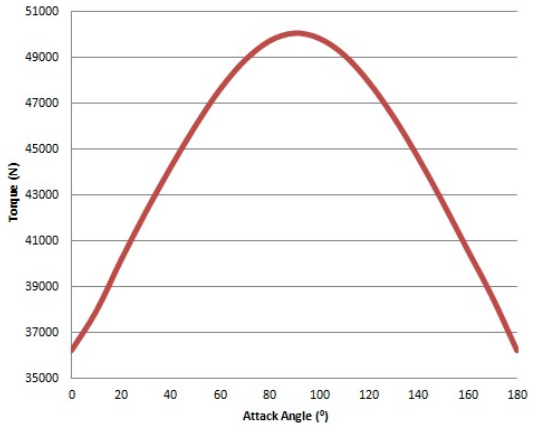

Figure 12. Torque at 30^0 support arm angle

Torque distribution for different support arm angles are also obtained. Figure 13 shows torque dependence on angle of attack when support arm angle changes. The curves represent torque distribution when the support arm angle changes

from 0^0 (bottom curve) to 90^0 (top curve) with 10^0 increments. It shows that the torque increases as the support arm angle increases and peaks out at the 90^0 support arm angle for any given angle of attack. Figure 14 shows similar pattern when the support arm angles increase further from 90^0 to 180^0. The curve on the top represents torque distribution at 90^0 support arm angle, and the curve further down represents 10 degrees more support arm angle with the 180^0 case at the bottom of the graph. All the curves also show a peak torque when the angle of attack is 90^0.

Figure 15 shows a comparison of torque distributions for wind speed of 20m/s, 15m/s, 10m/s, and 5m/s at the support arm angle of 30^0. It shows that the gain of torque due to higher wind speed is insignificant. It is also noticed that wind speed has no effect on torque distribution pattern.

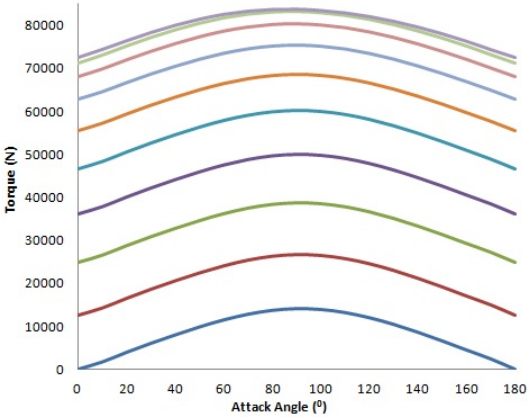

Figure 13. Torque at $0^0 \sim 90^0$ support arm angle

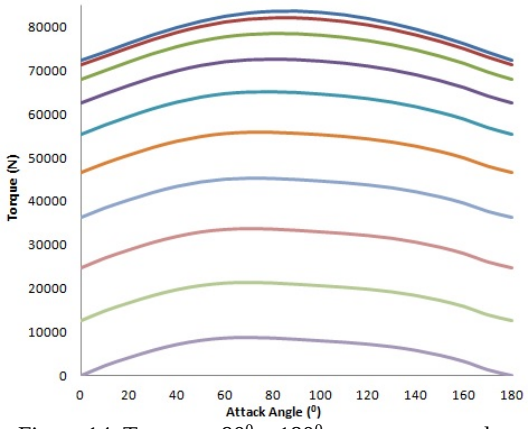

Figure 14. Torque at $90^0 \sim 180^0$ support arm angle

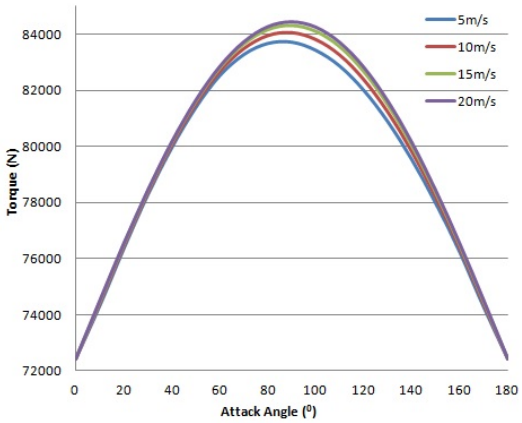

Figure 15. Effects of wind speed

5. Conclusions

From the results presented in section 4 for combined angle of attack (thus airfoil pivot angle), support arm angle, and four wind speed conditions, the following conclusions are drawn:

- Torque with respect to the rotation center of a VAWT depends on wind angle of attack and support arm position.
- Wind speed has insignificant effects on both torque magnitude and distribution pattern.
- For the NACA 0012 airfoil investigated in this study, the torque always peaks out at 90^0 angle of attack at any given support arm position. A control mechanism to maintain the airfoil at a constant 90^0 angle of attack is the optimal pattern for maximum efficiency and energy production.

The data presented in this study provide a guideline for pitch control design of this type of VAWT made with NACA0012 airfoil. The goal is to achieve higher efficiency than fixed airfoil VAWT, and thus more energy production. The results presented in this paper is only for 2-D models with single airfoil. A practical VAWT is typically constructed by using two or more airfoils. Factors such as number of airfoils, support arms, and wake generated when wind passing through one airfoil could affect another airfoil differently since the wind flow is assumed to be unidirectional in this study.

The symmetry shown in the results is likely due to the fact that NACA0012 airfoil does have a symmetric contour with respect to its chord. Other NACA airfoil with non-symmetric contour shall be compared.

6. References

1. A.R. Jha, Wind turbine technology, *CRC Press* (2010)
2. US Patent 1835018
3. H.M. Drees, The cycloturbine and its potential for broad application, *2nd International Symposium on Wind Energy*, Amsterdam, Netherlands, Oct., (1978)
4. M.H. Khan, Model and prototype performance characteristics of Savonius rotor windmill, *Wind Engineering*, Vol. 2, No 2, p75-85, (1978)
5. R.D. Mcconnell, Giromill Overview, *Wind Energy Innovative Systems Conference*, Colorado Springs, CO, May, (1979)
6. US Patent 7,344,353 B2
7. B.K. Kirke, L, Lazauskas, Enhancing the performance of a vertical axis wind turbine using a simple variable pitch system, *Wind Engineering*, Vol. 15, No. 4, P 187-195, (1991)
8. L. Lazauskas, B.K. Kirke, Performance optimization of a self-acting variable pitch vertical axis wind turbine, *Wind Engineering*, Vol. 16, No. 1, P 10-26, (1992)
9. L. Lazauskas, Three pitch control systems for vertical axis wind turbines compared, *Wind Engineering*, Vol. 16, No. 5, P 269-282, (1992)
10. P. Bhatta, M.A. Paluszek, J.B. Mueller, Individual blade pitch and camber control for vertical axis wind turbines, *Proc. World Wind Energy*, (2008)